

PREDATOR: Registration of 3D Point Clouds with Low Overlap

Shengyu Huang* Zan Gojcic* Mikhail Usvyatsov Andreas Wieser Konrad Schindler

ETH Zurich

{firstname.lastname@geod.baug.ethz.ch}

Abstract

We introduce PREDATOR, a model for pairwise **point-cloud registration** with **deep attention** to the **overlap region**. Different from previous work, our model is specifically designed to handle (also) point-cloud pairs with low overlap. Its key novelty is an overlap-attention block for early information exchange between the latent encodings of the two point clouds. In this way the subsequent decoding of the latent representations into per-point features is conditioned on the respective other point cloud, and thus can predict which points are not only salient, but also lie in the overlap region between the two point clouds. The ability to focus on points that are relevant for matching greatly improves performance: PREDATOR raises the rate of successful registrations by more than 20% in the low-overlap scenario, and also sets a new state of the art for the 3DMatch benchmark with 89% registration recall. Source code and pre-trained models will be available at <https://github.com/ShengyuH/OverlapPredator>.

1. Introduction

Recent work has made substantial progress in fully automatic, 3D feature-based point cloud registration. At first glance, benchmarks like 3DMatch [48] appear to be saturated, with multiple state-of-the-art (SOTA) methods [15, 7, 3] reaching nearly 95% feature matching recall and successfully registering >80% of all scan pairs. One may get the impression that the registration problem is solved—but this is actually not the case. We argue that the high success rates are a consequence of lenient evaluation protocols. We have been making our task too easy: existing literature and benchmarks [4, 48, 20] consider only pairs of point clouds with $\geq 30\%$ overlap to measure performance. Yet, the low-overlap regime is very relevant for practical applications. On the one hand, it may be difficult to ensure high overlap, for instance when moving along narrow corridors, or when

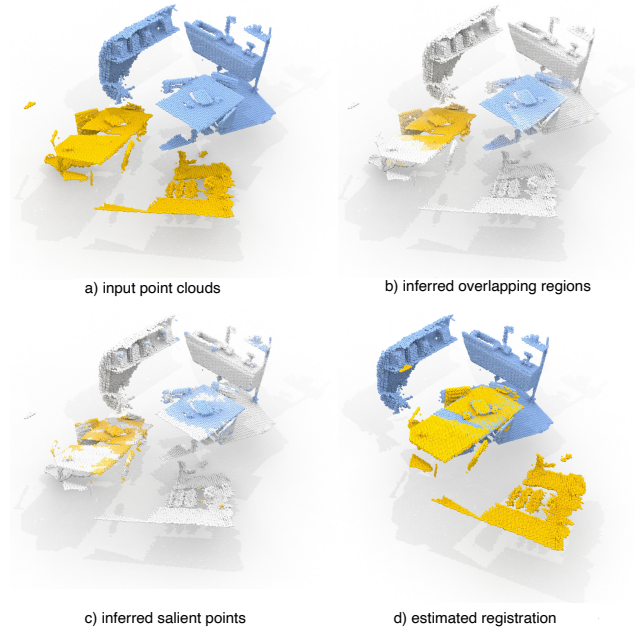


Figure 1: PREDATOR is designed to focus attention on the overlap region, and to prefer salient points in that region, so as to enable robust registration in spite of low overlap.

closing loops in the presence of occlusions (densely built-up areas, forest, etc.). On the other hand, data acquisition is often costly, so practitioners aim for a low number of scans with only the necessary overlap.

Driven by the evaluation protocol, the high-overlap scenario became the focus of research, whereas the more challenging low-overlap examples were largely neglected (*cf.* Fig. 1). As a consequence, the registration performance of even the best known methods deteriorates rapidly when the overlap between the two point clouds falls below 30%, see Fig. 2. Human operators, in contrast, can still register such low overlap point clouds without much effort.

This discrepancy is the starting point of the present work. To study its reasons, we have constructed a low-overlap

*First two authors contributed equally to this work.

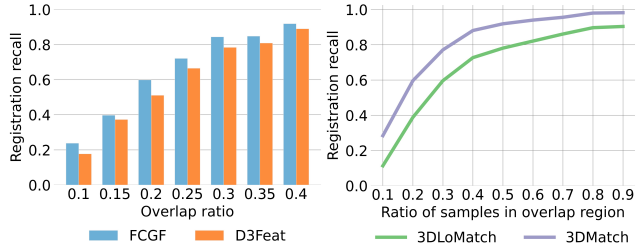


Figure 2: Registration with SOTA methods deteriorates rapidly for pairs with $<30\%$ overlap (left). By increasing the fraction of points sampled in the overlap region, many failures can be avoided as shown here for FCGF [7] (right).

dataset *3DLoMatch* (Sec. 4.1) from scans of the popular *3DMatch* benchmark, and have analysed the individual modules/steps of the registration pipeline (Fig. 2). It turns out that the effective receptive field of modern (fully convolutional) feature point descriptors [7, 3] is local enough and the descriptors are hardly corrupted by non-overlapping parts of the scans. Rather than coming up with yet another way to learn better descriptors, the key to registering low overlap point clouds is *learning where to look for feature points* (Fig. 2, right). A large performance boost can be achieved if the feature points are predominantly sampled from the overlapping portions of the scans.

We follow this path and introduce PREDATOR, a neural architecture for pairwise 3D point cloud registration that learns to (implicitly) detect the overlap region between two unregistered scans, and to focus on that region when extracting salient feature points. The main contributions of our work are:

- an analysis why existing registration architectures break down in the low-overlap regime
- a novel *overlap attention* block that allows for early information exchange between the two point clouds and focuses the subsequent steps on the overlap region
- a scheme to refine the feature point descriptors, by conditioning them also on the respective other point cloud
- a novel loss function to train *matchability* scores, which help to sample better and more repeatable interest points

Moreover, we make available the *3DLoMatch* dataset, containing the previously ignored scan pairs of *3DMatch* that have low (10-30%) overlap. In our experiments, PREDATOR greatly outperforms existing methods in the low-overlap regime, increasing registration recall by >10 percent points. It also sets a new state of the art for the conventional *3DMatch* benchmark, reaching a registration recall of 89%.

2. Related work

Local 3D feature descriptors: Early local descriptors for point clouds [19, 29, 28, 36, 35] aimed to characterise the local geometry by using hand-crafted features. While often

lacking robustness against clutter and occlusions, they have long been a default choice for downstream tasks because they naturally generalise across datasets [17]. In the last years, learned 3D feature descriptors have taken over and now routinely outperform their hand-crafted counterparts.

The pioneering 3DMatch method [48] is based on a Siamese 3D CNN that extracts local feature descriptors from a signed distance function embedding. Others [20, 16] first extract hand-crafted features, then map them to a compact representation using multi-layer perceptrons. PPFNet [10], and its self-supervised version PPF-FoldNet [9], combine point pair features with a PointNet [26] architecture to extract descriptors that are aware of the global context. To alleviate artefacts caused by noise and voxelisation, [15] proposed to use a smoothed density voxel grid as input to a 3D CNN. These early works achieved strong performance, but still operate on individual local patches, which greatly increases the computational cost and limits the receptive field to a predefined size.

Fully convolutional architectures [22] that enable dense feature computation over the whole input in a single forward pass [11, 12, 27] have been adopted to design faster 3D feature descriptors. Building on sparse convolutions [6], FCGF [7] achieves a performance similar to the best patch-based descriptors [15], while being orders of magnitude more efficient. D3Feat [3] complements a fully convolutional feature descriptor with an interest point detector trained to detect salient points.

Contextual information: In the traditional pipeline, feature extraction is done independently per point cloud. Information is only mixed when computing pairwise similarities, although aggregating contextual information at an earlier stage could provide additional cues to robustify the descriptors and guide the matching step.

In 2D feature learning, [43] use an attention mechanism in the bottleneck of an encoder-decoder scheme to aggregate the contextual information, which is later used to condition the output of the decoder on the second image. SuperGlue [30] infuses the contextual information into the learned descriptors with a whole series of self- and cross-attention layers, built upon the message-passing GNN. Early information mixing was previously also explored in the field of deep point cloud registration, where [40, 41] use a transformer module to extract task-specific 3D features that are reinforced with contextual information.

Interest point sampling: The classic principle to sample salient rather than random points has also found its way into learned 2D [11, 12, 27, 43] and 3D [46, 3] local feature extraction. All these methods implicitly assume that the saliency of a point fully determines its utility for downstream tasks. Here, we take a step back and argue that, while saliency is desirable for an interest point, it is not sufficient on its own. Indeed, in order to contribute to registration a

point should not only be salient, but must also lie in the region where the two point clouds overlap—an essential property that, surprisingly, has largely been neglected thus far.

Deep point-cloud registration: Instead of combining learned feature descriptors with some off-the-shelf robust optimization at inference time, a parallel stream of work aims to embed the (differentiable) estimation of the transformation parameters into the learning pipeline. PointNetLK [1] combines a PointNet-based global feature descriptor [26] with a Lucas/Kanade-like optimization algorithm [23] and estimates the relative transformation in an iterative fashion. DCP [40] uses a DGCNN network [42] to extract local features and computes soft correspondences before using the Kabsch algorithm to estimate the transformation parameters. To relax the need for strict one-to-one correspondence, DCP was later extended to PRNet [41], which includes a keypoint detection step and allows for partial correspondence. Instead of simply using soft correspondences, [47] estimate the similarity matrix with a differentiable Sinkhorn layer [32]. Similar to other methods, the weighted Kabsch algorithm [2] is used in [47] to estimate the transformation parameters. Finally, [14, 5] complement a learned feature descriptor with an outlier filtering network, which infers the points’ influence weights for later use in the weighted Kabsch algorithm.

3. Method

PREDATOR is a two-stream encoder-decoder network. Our implementation uses residual blocks with KPConv-style point convolutions [34], but the architecture is agnostic w.r.t. the backbone and could also be implemented with other formulations of 3D convolutions, such as for instance sparse voxel convolutions [6]. The architecture of PREDATOR can be decomposed into three main modules:

1. encoding of the two point clouds into smaller sets of superpoints and associated latent feature encodings, with shared weights (Sec. 3.2);
2. the overlap attention module (in the bottleneck) that extracts co-contextual information between the feature encodings of the two point clouds, and assigns each superpoint two overlap scores that quantify how likely the superpoint itself and its soft-correspondence are located in the overlap between the two inputs (Sec. 3.3);
3. decoding of the mutually conditioned bottleneck representations to point-wise descriptors as well as refined per-point overlap and matchability scores (Sec. 3.4).

Before diving into each component we lay out the basic problem setting and notation in Sec. 3.1.

3.1. Problem setting

Consider two point clouds $\mathbf{P} = \{\mathbf{p}_i \in \mathbb{R}^3 | i = 1..N\}$, and $\mathbf{Q} = \{\mathbf{q}_i \in \mathbb{R}^3 | i = 1..M\}$. Our goal is to recover a

rigid transformation $T_{\mathbf{P}}^{\mathbf{Q}}$ with parameters $\mathbf{R} \in SO(3)$ and $\mathbf{t} \in \mathbb{R}^3$ that aligns \mathbf{P} to \mathbf{Q} . By a slight abuse of notation we use the same symbols for sets of points and for their corresponding matrices $\mathbf{P} \in \mathbb{R}^{N \times 3}$ and $\mathbf{Q} \in \mathbb{R}^{M \times 3}$.

Obviously $T_{\mathbf{P}}^{\mathbf{Q}}$ can only ever be determined from the data if \mathbf{P} and \mathbf{Q} have sufficient overlap, meaning that after applying the ground truth transformation $\bar{T}_{\mathbf{P}}^{\mathbf{Q}}$ the overlap ratio

$$\frac{1}{N} |\{ \|\bar{T}_{\mathbf{P}}^{\mathbf{Q}}(\mathbf{p}_i) - \text{NN}(\bar{T}_{\mathbf{P}}^{\mathbf{Q}}(\mathbf{p}_i), \mathbf{Q})\|_2 \leq v \}| > \tau, \quad (1)$$

where NN denotes the nearest-neighbour operator w.r.t. its second argument, $\|\cdot\|_2$ is the Euclidean norm, $|\cdot|$ is the set cardinality, and v is a tolerance that depends on the point density.² Contrary to previous work [48, 20], where the threshold to even attempt the alignment is typically $\tau > 0.3$, we are interested in low-overlap point clouds with $\tau > 0.1$.

3.2. Encoder

We follow [34] and first preprocess raw point clouds with grid-based subsampling, such that \mathbf{P} and \mathbf{Q} have reasonably uniform point density. In the shared encoder, a series of ResNet-like blocks and strided convolutions aggregate the raw points into *superpoints* $\mathbf{P}' \in \mathbb{R}^{N' \times 3}$ and $\mathbf{Q}' \in \mathbb{R}^{M' \times 3}$ with associated features $\mathbf{X}^{\mathbf{P}'} \in \mathbb{R}^{N' \times b}$ and $\mathbf{X}^{\mathbf{Q}'} \in \mathbb{R}^{M' \times b}$. Note that superpoints correspond to a fixed receptive field, so their number depends on the spatial extent of the input point cloud and may be different for the two inputs.

3.3. Overlap attention module

So far, the features $\mathbf{X}^{\mathbf{P}'}$, $\mathbf{X}^{\mathbf{Q}'}$ in the bottleneck encode the geometry and context of the two point clouds. But $\mathbf{X}^{\mathbf{P}'}$ has no knowledge of point cloud \mathbf{Q} and vice versa. In order to reason about their respective overlap regions, some cross-talk is necessary. We argue that it makes sense to add that cross-talk at the level of superpoints in the bottleneck, just like a human operator will first get a rough overview of the overall shape to determine likely overlap regions, and only after that identifies precise feature points in those regions.

Graph convolutional neural network: Before connecting the two feature encodings, we first further aggregate and strengthen their contextual relations individually with a graph neural network (GNN) [42]. In the following, we describe the GNN for point cloud \mathbf{P}' . The GNN for \mathbf{Q}' is the same. First, the superpoints in \mathbf{P}' are linked into a graph in Euclidean space with the k -NN method. Let $\mathbf{x}_i \in \mathbb{R}^b$ denote the feature encoding of superpoint \mathbf{p}'_i , and $(i, j) \in \mathcal{E}$ the graph edge between superpoints \mathbf{p}'_i and \mathbf{p}'_j . The encoder features are then iteratively updated as

$$^{(k+1)}\mathbf{x}_i = \max_{(i,j) \in \mathcal{E}} h_{\theta}(\text{cat}[^{(k)}\mathbf{x}_i, ^{(k)}\mathbf{x}_j - ^{(k)}\mathbf{x}_i]), \quad (2)$$

²For efficiency, v is in practice determined after voxel-grid downsampling of the two point clouds.

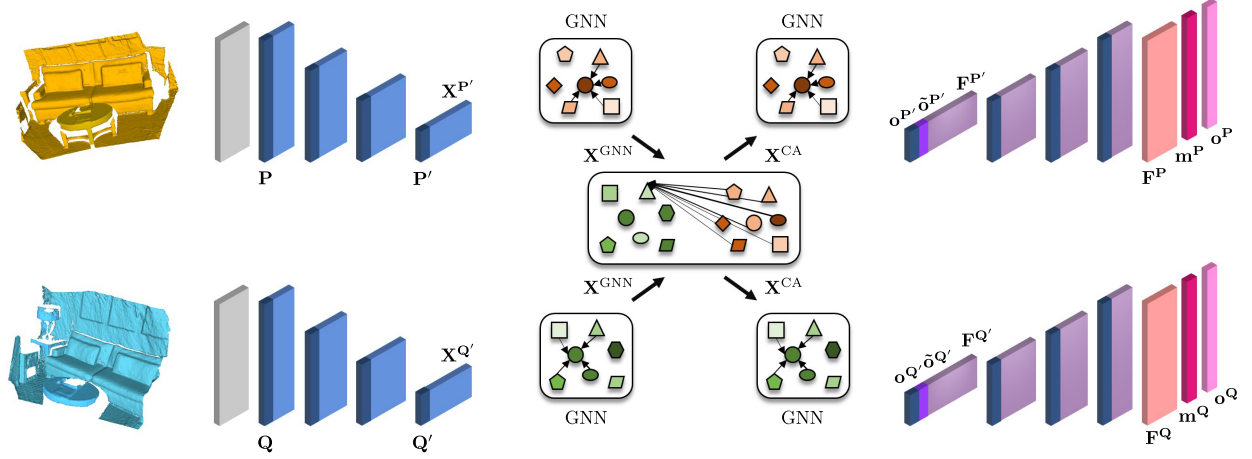


Figure 3: Network architecture of PREDATOR. Voxel-gridded point clouds \mathbf{P} and \mathbf{Q} are fed to the encoder, which extracts the superpoints \mathbf{P}' and \mathbf{Q}' and their latent features $\mathbf{X}^{\mathbf{P}'}$, $\mathbf{X}^{\mathbf{Q}'}$. The overlap-attention module updates the features with co-contextual information in a series of self- (GNN) and cross-attention (CA) blocks, and projects them to overlap $\mathbf{o}^{\mathbf{P}'}$, $\mathbf{o}^{\mathbf{Q}'}$ and cross-overlap $\tilde{\mathbf{o}}^{\mathbf{P}'}$, $\tilde{\mathbf{o}}^{\mathbf{Q}'}$ scores. Finally, the decoder transforms the conditioned features and overlap scores to per-point feature descriptors $\mathbf{F}^{\mathbf{P}}$, $\mathbf{F}^{\mathbf{Q}}$, overlap scores $\mathbf{o}^{\mathbf{P}}$, $\mathbf{o}^{\mathbf{Q}}$, and matchability scores $\mathbf{m}^{\mathbf{P}}$, $\mathbf{m}^{\mathbf{Q}}$.

where $h_\theta(\cdot)$ denotes a linear layer followed by instance normalization [37] and a LeakyReLU activation [24], $\max(\cdot)$ denotes element-/channel-wise max-pooling, and $\text{cat}[\cdot, \cdot]$ means concatenation. This update is performed twice with separate (not shared) parameters θ , and the final GNN features $\mathbf{x}_i^{\text{GNN}} \in \mathbb{R}^{d_b}$ are obtained as

$$\mathbf{x}_i^{\text{GNN}} = h_\theta(\text{cat}[(^{(0)}\mathbf{x}_i, ^{(1)}\mathbf{x}_i, ^{(2)}\mathbf{x}_i)]) . \quad (3)$$

Cross-attention block: Knowledge about potential overlap regions can only be gained by mixing information about both point clouds. To this end we adopt a cross-attention block [30] based on the message passing formulation [13]. First, each superpoint in \mathbf{P}' is connected to all superpoints in \mathbf{Q}' to form a bipartite graph. Inspired by the Transformer architecture [39], vector-valued keys $\mathbf{k}_j \in \mathbb{R}^b$ and queries $\mathbf{s}_i \in \mathbb{R}^b$ are learned for each superpoint and used to retrieve (also learned) values $\mathbf{v}_j \in \mathbb{R}^b$. The messages are then computed as weighted averages of the values,

$$\mathbf{m}_{i \leftarrow} = \sum_{j: (i, j) \in \mathcal{E}} a_{ij} \mathbf{v}_j , \quad (4)$$

with attention weights $a_{ij} = \text{softmax}(\mathbf{s}_i^T \mathbf{k}_j / \sqrt{b})$ [30]. I.e., to update a superpoint \mathbf{p}'_i one combines that point's query with the keys and values of all superpoints \mathbf{q}'_j . The queries, keys, and values are linear projections of the corresponding features $\mathbf{x}_i^{\text{GNN}}$, $\mathbf{x}_j^{\text{GNN}}$. In line with the literature, in practice we use a multi-attention layer with four parallel attention heads [39]. The co-contextual features are computed as

$$\mathbf{x}_i^{\text{CA}} = \mathbf{x}_i^{\text{GNN}} + \text{MLP}(\text{cat}[\mathbf{x}_i^{\text{GNN}}, \mathbf{m}_{i \leftarrow}]) , \quad (5)$$

with $\text{MLP}(\cdot)$ denoting a three-layer fully connected network with instance normalization [37] and ReLU [25] ac-

tivations after the first two layers. The same cross-attention block is also applied in reverse direction, so that information flows in both directions, $\mathbf{P}' \rightarrow \mathbf{Q}'$ and $\mathbf{Q}' \rightarrow \mathbf{P}'$.

Overlap scores of the bottleneck points: The above update with co-contextual information is done for each superpoint in isolation, without considering the local context within each point cloud. We therefore, explicitly update the local context after the cross-attention block using another GNN that has the same architecture and underlying graph (within-point cloud links) as above, but separate parameters θ . This yields the final latent feature encodings $\mathbf{F}^{\mathbf{P}'} \in \mathbb{R}^{N' \times b}$ and $\mathbf{F}^{\mathbf{Q}'} \in \mathbb{R}^{M' \times b}$, which are now conditioned on the features of the respective other point cloud. Those features are linearly projected to overlap scores $\mathbf{o}^{\mathbf{P}'} \in \mathbb{R}^{N'}$ and $\mathbf{o}^{\mathbf{Q}'} \in \mathbb{R}^{M'}$, which can be interpreted as probabilities that a certain superpoint lies in the overlap region. Additionally, one can compute *soft correspondences* between superpoints and from the correspondence weights predict the *cross-overlap score* of a superpoint \mathbf{p}'_i , i.e., the probability that its correspondence in \mathbf{Q}' lies in the overlap region:

$$\tilde{o}_i^{\mathbf{P}'} := \mathbf{w}_i^T \mathbf{o}^{\mathbf{Q}'}, \quad w_{ij} := \text{softmax}\left(\frac{1}{t} \langle \mathbf{f}_i^{\mathbf{P}'}, \mathbf{f}_j^{\mathbf{Q}'} \rangle\right) , \quad (6)$$

where $\langle \cdot, \cdot \rangle$ is the inner product, and t is the temperature parameter that controls the soft assignment. In the limit $t \rightarrow 0$, Eq. (6) converges to hard nearest-neighbour assignment.

3.4. Decoder

Our decoder starts from conditioned features $\mathbf{F}^{\mathbf{P}'}$, concatenates them with the overlap scores $\mathbf{o}^{\mathbf{P}'}$, $\tilde{\mathbf{o}}^{\mathbf{P}'}$, and outputs per-point feature descriptors $\mathbf{F}^{\mathbf{P}} \in \mathbb{R}^{N \times 32}$ and refined per-point overlap and matchability scores $\mathbf{o}^{\mathbf{P}}$, $\mathbf{m}^{\mathbf{P}} \in \mathbb{R}^N$.

The matchability can be seen as a "conditional saliency" that quantifies how likely a point is to be matched correctly, given the points (resp. features) in the other point cloud \mathbf{Q} .

The decoder architecture combines NN-upsampling with 4 PointNet-style MLP layers [26], and includes skip connections from the corresponding encoder layers. We deliberately keep the overlap score and the matchability separate to disentangle the reasons why a point is a good/bad candidate for matching: in principle a point can be unambiguously matchable but lie outside the overlap region, or it can lie in the overlap but have an ambiguous descriptor. Empirically, we find that the network learns to predict high matchability mostly for points in the overlap; probably reflecting the fact that the ground truth correspondences used for training, naturally, always lie in the overlap. For further details about the architecture, please refer to Sec. A.3 and the source code.

3.5. Loss function and training

PREDATOR is trained end-to-end, using three losses w.r.t. ground truth correspondences as supervision.

Circle loss: To supervise the point-wise feature descriptors we follow³ [3] and use the circle loss [33], a variant of the more common triplet loss. Consider again a pair of overlapping point clouds \mathbf{P} and \mathbf{Q} , this time aligned with the ground truth transformation. We start by extracting the points $\mathbf{p}_i \in \mathbf{P}_p \subset \mathbf{P}$ that have at least one (possibly multiple) correspondence in \mathbf{Q} , where the set of correspondences $\mathcal{E}_p(\mathbf{p}_i)$ is defined as points in \mathbf{Q} that lie within a radius r_p around \mathbf{p}_i . Similarly, all points of \mathbf{Q} outside a (larger) radius r_s form the set of negatives $\mathcal{E}_n(\mathbf{p}_i)$. The circle loss is then computed from n_p points sampled randomly from \mathbf{P}_p :

$$\mathcal{L}_c^{\mathbf{P}} = \frac{1}{n_p} \sum_{i=1}^{n_p} \log \left[1 + \sum_{j \in \mathcal{E}_p} e^{\beta_p^j (d_i^j - \Delta_p)} \cdot \sum_{k \in \mathcal{E}_n} e^{\beta_n^k (\Delta_n - d_i^k)} \right], \quad (7)$$

where $d_i^j = \|\mathbf{f}_{\mathbf{p}_i} - \mathbf{f}_{\mathbf{q}_j}\|_2$ denotes distance in feature space, and Δ_n, Δ_p are negative and positive margins, respectively. The weights $\beta_p^j = \gamma(d_i^j - \Delta_p)$ and $\beta_n^k = \gamma(\Delta_n - d_i^k)$ are determined individually for each positive and negative example, using the empirical margins $\Delta_p := 0.1$ and $\Delta_n := 1.4$ with hyper-parameter γ . The reverse loss $\mathcal{L}_c^{\mathbf{Q}}$ is computed in the same way, for a total circle loss $\mathcal{L}_c = \frac{1}{2}(\mathcal{L}_c^{\mathbf{P}} + \mathcal{L}_c^{\mathbf{Q}})$.

Overlap loss: The estimation of the overlap probability is cast as binary classification and supervised using the overlap loss $\mathcal{L}_o = \frac{1}{2}(\mathcal{L}_o^{\mathbf{P}} + \mathcal{L}_o^{\mathbf{Q}})$, where

$$\mathcal{L}_o^{\mathbf{P}} = \frac{1}{|\mathbf{P}|} \sum_{i=1}^{|\mathbf{P}|} \bar{o}_{\mathbf{p}_i} \log(o_{\mathbf{p}_i}) + (1 - \bar{o}_{\mathbf{p}_i}) \log(1 - o_{\mathbf{p}_i}). \quad (8)$$

The ground truth label $\bar{o}_{\mathbf{p}_i}$ of point \mathbf{p}_i is defined as

$$\bar{o}_{\mathbf{p}_i} = \begin{cases} 1, & \|\bar{T}_{\mathbf{P}}^{\mathbf{Q}}(\mathbf{p}_i) - \text{NN}(\bar{T}_{\mathbf{P}}^{\mathbf{Q}}(\mathbf{p}_i), \mathbf{Q})\|_2 < r_o \\ 0, & \text{otherwise} \end{cases}, \quad (9)$$

with overlap threshold r_o . The reverse loss $\mathcal{L}_o^{\mathbf{Q}}$ is computed in the same way. The contributions from positive and negative examples are balanced with weights inversely proportional to their relative frequencies.

Matchability loss: Supervising the matchability scores is a bit more difficult, as it is not clear in advance which are the right points to take into account during correspondence search. We follow a simple intuition: good keypoints are those that can be matched successfully at a given point during training, with the current feature descriptors. Hence, we cast the prediction as binary classification and generate the ground truth labels on the fly. Again, we sum the two symmetric losses, $\mathcal{L}_m = \frac{1}{2}(\mathcal{L}_m^{\mathbf{P}} + \mathcal{L}_m^{\mathbf{Q}})$, with

$$\mathcal{L}_m^{\mathbf{P}} = \frac{1}{|\mathbf{P}|} \sum_{i=1}^{|\mathbf{P}|} \bar{m}_{\mathbf{p}_i} \log(m_{\mathbf{p}_i}) + (1 - \bar{m}_{\mathbf{p}_i}) \log(1 - m_{\mathbf{p}_i}), \quad (10)$$

where ground truth labels $\bar{m}_{\mathbf{p}_i}$ are computed on the fly via nearest neighbour search $\text{NN}_{\mathbf{F}}(\cdot, \cdot)$ in feature space:

$$\bar{m}_{\mathbf{p}_i} = \begin{cases} 1, & \|\bar{T}_{\mathbf{P}}^{\mathbf{Q}}(\mathbf{p}_i) - \text{NN}_{\mathbf{F}}(\bar{T}_{\mathbf{P}}^{\mathbf{Q}}(\mathbf{p}_i), \mathbf{Q})\|_2 < r_m \\ 0, & \text{otherwise.} \end{cases} \quad (11)$$

Implementation and training: PREDATOR is implemented in pytorch. For the *3DMatch* dataset, we train for 30 epochs, using SGD with initial learning rate 0.005, momentum 0.98, and weight decay 10^{-6} . The learning rate is exponentially decayed by 0.05 after each epoch. Due to memory constraints we use batch size 1 in all experiments and sample at most $n_p = 256$ positive pairs for the circle loss. Data augmentation includes random rotations $\in [0^\circ, 360^\circ]$ around all three axes and Gaussian noise with $\sigma = 0.5$ cm, added independently to each coordinate. At the start of the training we supervise PREDATOR only with the circle and overlap losses, the matchability loss is added only after few epochs, when the point-wise features are already meaningful (i.e., $>30\%$ of all points in \mathbf{P}_p can be matched correctly). The three loss terms are weighted equally. The hyper-parameters are set relative to the voxel size V of the initial grid subsampling (respectively, the average point-to-point distance). For the circle loss, the positive radius r_p is set to $1.5 \cdot V$, and the safe radius is set to $4 \cdot V$. For the overlap loss, r_o is also set to $1.5 \cdot V$ and r_m is set to be $2 \cdot V$, in accordance with the distance threshold for a valid correspondence in the subsequent RANSAC pose estimation. The training settings for the *ModelNet* dataset are given in Sec. A.4.

³ Added to the repository after publication, not mentioned in the paper.

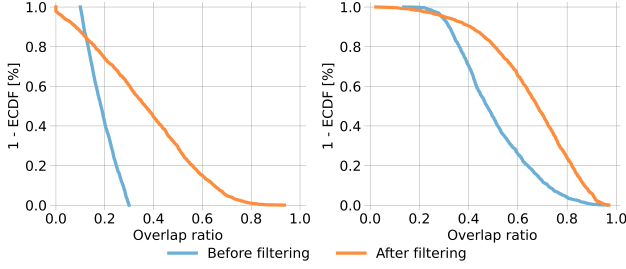


Figure 4: Distribution of the relative overlap ratio before and after filtering the points with the inferred overlap scores, *3DLoMatch* (left) and *3DMatch* (right).

4. Experiments

We evaluate PREDATOR and justify our design choices on real scan data, using *3DMatch* and *3DLoMatch*. Additionally, we compare PREDATOR to direct registration methods on the synthetic, object-centric *ModelNet40*.

4.1. Datasets and preprocessing

3DMatch/3DLoMatch: The official *3DMatch* dataset [48] considers only scan pairs with $>30\%$ overlap. Here, we add its counterpart that considers only scan pairs with overlaps between 10 and 30% and call this collection *3DLoMatch*⁴. For both datasets we stick to the accepted split into 54 training and 8 test scenes.

ModelNet40: [44] contains 12,311 CAD models of man-made objects from 40 different categories. We follow [47] and use 5,112 samples for training and 1,202 samples for validation, from the first 20 categories. We then test on 1,266 samples from the other 20 categories. Like [47], we randomly sample planes that cut away 30% of the points, to obtain point clouds with 70% completeness and, on average, 73.5% pairwise overlap. For our purposes we additionally run a version where we cut away 50% of the points, to obtain a second test set with 53.6% average overlap, which we call *ModelLoNet* (lower overlap is not meaningful, due to the low number of points per model).

4.2. Evaluation metrics

We use the standard metrics of *3DMatch* to assess the performance of PREDATOR and to compare it to three state-of-the-art methods: 3DSN [15], FCGF [7] and 3DFeat [3]. Our main metric, corresponding to the actual aim of point cloud registration, is *Registration Recall* (*RR*), i.e., the fraction of scan pairs for which the correct transformation parameters are found with RANSAC. Following the literature, we also report *Feature Match Recall* (*FMR*), defined as the fraction of pairs that have $>5\%$ "inlier" matches with <10 cm residual under the ground truth transforma-

⁴Due to a bug in the official implementation of the overlap computation for *3DMatch*, a few ($<7\%$) scan pairs are included in both datasets.

# Samples (k)	<i>3DMatch</i>					<i>3DLoMatch</i>				
	5000	2500	1000	500	250	5000	2500	1000	500	250
<i>Inlier ratio (%)</i>										
rand	43.6	41.5	36.7	31.9	25.9	15.7	14.7	12.8	10.9	8.7
top-k (<i>om</i>)	61.0	67.3	71.8	73.1	73.1	26.0	31.4	36.0	37.4	38.0
filt. (<i>o</i>) + prob. (<i>m</i>)	<u>55.2</u>	<u>55.2</u>	<u>53.7</u>	<u>51.3</u>	<u>46.4</u>	<u>24.7</u>	<u>25.0</u>	<u>24.8</u>	<u>24.0</u>	<u>22.7</u>
prob. (<i>om</i>)	49.9	50.3	49.2	46.3	41.8	20.0	20.8	21.0	20.2	19.0
<i>Registration Recall (%)</i>										
rand	83.9	82.9	81.5	79.9	69.9	39.3	38.8	36.9	30.3	23.2
top-k (<i>om</i>)	81.6	84.3	80.2	72.6	60.3	54.6	52.4	45.7	38.1	28.9
filt. (<i>o</i>) + prob. (<i>om</i>)	<u>85.7</u>	<u>84.4</u>	<u>86.6</u>	<u>86.3</u>	<u>83.3</u>	51.3	<u>53.3</u>	<u>54.6</u>	<u>54.4</u>	52.0
prob. (<i>om</i>)	88.3	88.3	89.0	88.4	84.7	<u>54.2</u>	55.8	56.7	56.1	<u>50.7</u>

Table 1: Performance of PREDATOR for different strategies of sampling the interest points; *o*, *m* and *om* denote overlap score, matchability score and their product, respectively.

tion (without checking if the transformation can be recovered from those matches), and *Inlier Ratio* (*IR*), the fraction of correct correspondences among the putative matches.

For *ModelNet40* we follow [47] and measure the performance using the *Relative Rotation Error* (*RRE*) (geodesic distance between estimated and GT rotation matrices), the *Relative Translation Error* (*RTE*) (Euclidean distance between the estimated and GT translations), and the *Chamfer distance* (*CD*) between the two scans after applying the estimated transformation. For more details please see Sec. A.1.

4.3. 3DMatch

Relative overlap ratio: We first evaluate if PREDATOR achieves its goal to focus on the overlap. We discard points with a predicted overlap score $o_i < 0.5$, compute the overlap ratio, and compare it to the one of the original scans. Fig. 4 shows that more than half of the low-overlap pairs are pushed over the 30% threshold that prior works considered the lower limit for registration. On average, discarding points with low overlap scores almost doubles the overlap in *3DLoMatch* (98% increase). Notably, it also increases the overlap in standard *3DMatch* by, on average, $>35\%$.

Interest point sampling: PREDATOR significantly increases the effective overlap, but does that improve downstream registration performance? To test this we use the overlap scores *o* and matchability scores *m* to bias interest point sampling. We compare three variants: *top-k* (*om*), where we multiply $o \cdot m$ and pick the top-*k* points according to the combined score; *prob.* (*om*), where we instead sample points with probability proportional to the combined score; and *filt. (o)+prob. (om)*, where we discard points with $o < 0.5$, then sample from the remaining ones proportional to *om*.

Tab. 1 shows that any of the informed sampling strategies greatly increases the *inlier ratio*, and as a consequence also the *registration recall*. The gains are larger when fewer points are sampled. In the low-overlap regime the inlier ratios more than triple for up to 1000 points. We observe that,

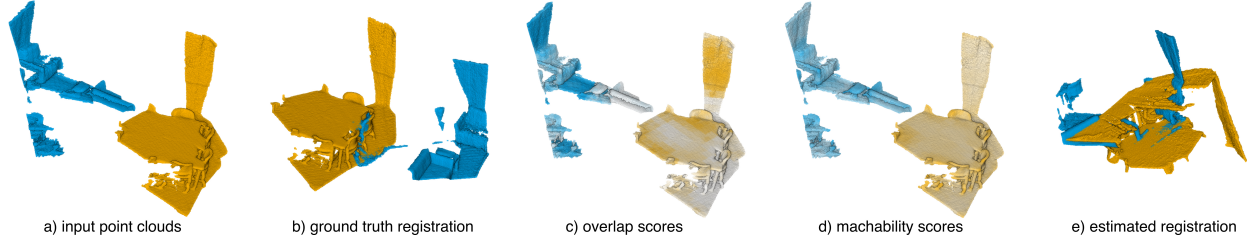


Figure 5: An extreme case where the overlap is insufficient for registration even with the proposed attention mechanism.

# Samples	3DMatch					3DLoMatch				
	5000	2500	1000	500	250	5000	2500	1000	500	250
<i>Feature Match Recall (%)</i>										
3DSN [15]	95.0	94.3	92.9	90.1	82.9	63.6	61.7	53.6	45.2	34.2
FCGF [7]	97.4	97.3	97.0	96.7	96.6	76.6	75.4	74.2	<u>71.7</u>	<u>67.3</u>
D3Feat [3]	95.6	95.4	94.5	94.1	93.1	67.3	66.7	67.0	66.7	66.5
Ours	<u>96.6</u>	<u>96.2</u>	<u>96.2</u>	<u>95.8</u>	<u>95.5</u>	<u>71.7</u>	<u>73.8</u>	<u>73.8</u>	72.9	72.3
<i>Inlier ratio (%)</i>										
3DSN [15]	36.0	32.5	26.4	21.5	16.4	11.4	10.1	8.0	6.4	4.8
FCGF [7]	56.8	54.1	<u>48.7</u>	<u>42.5</u>	34.1	21.4	<u>20.0</u>	<u>17.2</u>	<u>14.8</u>	11.6
D3Feat [3]	39.0	38.8	40.4	41.5	41.8	13.2	13.1	14.0	14.6	<u>15.0</u>
Ours	<u>49.9</u>	<u>50.3</u>	49.2	46.3	41.8	<u>20.0</u>	20.8	21.0	20.2	19.0
<i>Registration Recall (%)</i>										
3DSN [15]	78.4	76.2	71.4	67.6	50.8	33.0	29.0	23.3	17.0	11.0
FCGF [7]	<u>85.1</u>	<u>84.7</u>	83.3	81.6	71.4	<u>40.1</u>	41.7	38.2	35.4	26.8
D3Feat [3]	81.6	84.5	<u>83.4</u>	<u>82.4</u>	<u>77.9</u>	37.2	<u>42.7</u>	<u>46.9</u>	<u>43.8</u>	<u>39.1</u>
Ours	88.3	88.3	89.0	88.4	84.7	54.2	55.8	56.7	56.1	50.7

Table 2: Results on the 3DMatch and 3DLoMatch datasets, for different numbers of sampled interest points.

as expected, high inlier ratio does not necessarily imply high registration recall: our scores are apparently well calibrated, so that *top-k (om)* indeed finds most inliers, but these are often clustered and too close to each other to reliably estimate the transformation parameters. We thus use the more robust *prob. (om)* sampling, which yields the best *registration recall*. It may be possible to achieve even higher registration recall by combining *top-k (om)* sampling with non-maxima suppression. We leave this for future work.

Comparison to feature-based methods: We compare PREDATOR to recent feature-based registration methods (Tab. 2). For a more comprehensive assessment we follow [3] and report performance with different numbers of sampled interest points. Qualitative results are shown in Fig. 6. PREDATOR greatly outperforms existing methods on the low-overlap 3DLoMatch dataset, improving registration recall by 10-20 percent points (pp) over the closest competitor—variously FCGF or 3DFeat. Moreover, it also consistently reaches the highest registration recall on standard 3DMatch, showing that its attention to the overlap pays off even for scans with moderately large overlap. In line with our motivation, what matters is not so much the choice of descriptors, but finding interest points that lie in

<i>conditioned</i>	<i>cross-overlap score</i>	3DMatch			3DLoMatch		
		FMR	IR	RR	FMR	IR	RR
		<u>96.2</u>	47.2	86.9	<u>71.8</u>	<u>18.0</u>	50.9
✓		95.5	46.4	87.1	73.0	17.6	54.4
	✓	96.1	<u>47.8</u>	<u>87.3</u>	69.5	15.8	48.4
✓	✓	96.6	49.9	88.3	71.7	20.0	<u>54.2</u>

Table 3: Ablation of the network architecture design; *conditioned* denotes conditioning the bottleneck features on the respective other point cloud, *cross-overlap score* denotes that two overlap scores instead of one are appended to the features as input to the decoder.

the overlap region – especially if that region is small.

The results also support our claim that one should evaluate the complete registration pipeline: FCGF slightly beats PREDATOR in terms of *FMR*, except in the low-overlap, small sample regime. But PREDATOR mostly compensates that deficit when looking at the inlier ratio, i.e., a higher number of *potentially matchable* point pairs does not always translate to more usable *matches*⁵. Even in cases where the inlier ratio remains a bit below that of FCGF, our method achieves higher registration recall.

Comparison to direct registration methods: We tried to compare PREDATOR also to recent methods for direct registration of partial point clouds. Unfortunately, for both PR-Net [41] and RPM-Net [47], training on 3DMatch failed to converge to reasonable results, as already observed in [5]. It appears that their feature extraction is specifically tuned to synthetic, object-centric point clouds. Thus, in a further attempt we replaced the feature extractor of RPM-Net with FCGF. This brought the registration recall on 3DMatch to 54.9%, still far from the 85.1% that FCGF features achieve with RANSAC. We conclude that direct pairwise registration is at this point only suitable for geometrically simple objects in controlled settings like *ModelNet40*.

Ablation study: We ablate our point scoring functions in Tab. 3. By conditioning the decoder input on the respective other point cloud, registration recall increases only by 0.2 pp for 3DMatch, but by 3.3 pp for 3DLoMatch. Adding also the cross-overlap score brings a bigger gain of 1.2 pp

⁵See Tab. 1, where *top-k (om)* sampling has even higher inlier ratio than FCGF, yet lower registration performance.

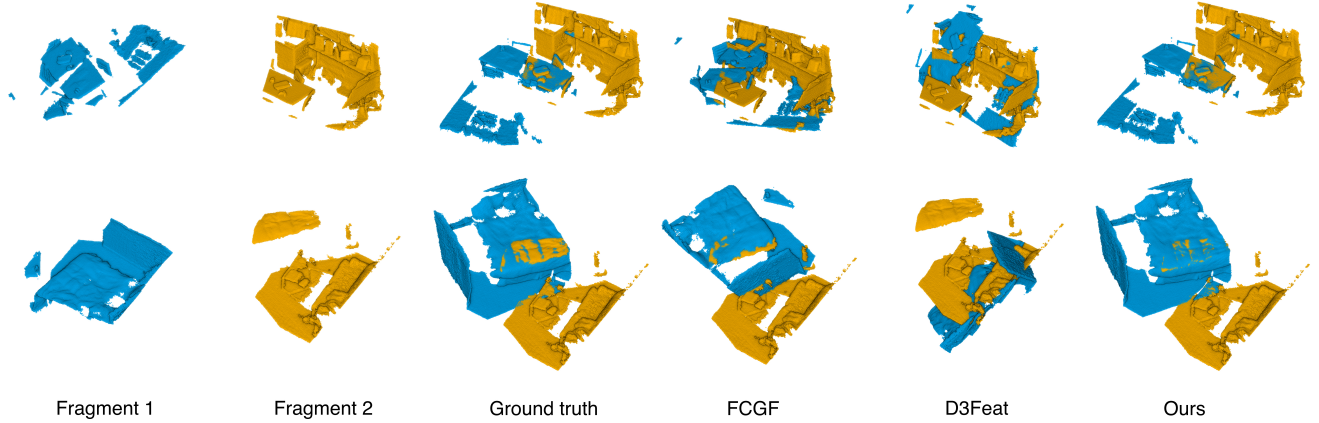


Figure 6: Example results of PREDATOR for the *3DLoMatch* dataset. Our model is able to register challenging low-overlap scan pairs with the proposed attention mechanism, while both FCGF[7] and D3Feat [3] fail.

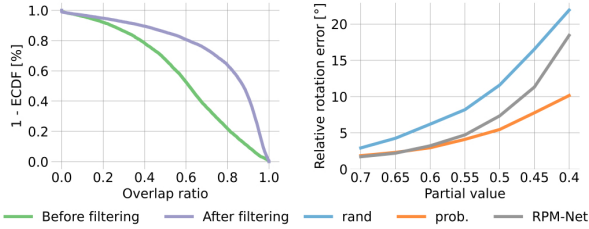


Figure 7: Improved relative overlap ratio after filtering the points with the inferred overlap scores on 8862 *ModelNet* partial scans (left). Owing to the improved overlap ratio, PREDATOR is robust to the changes of partial value p_v , while the performance of RPM-Net drops rapidly (right). *rand* and *prob.* denote the random and *prob. (om)* biased sampling of 450 interest points, respectively.

for *3DMatch*, but no further gain for *3DLoMatch*. For more ablation studies, please see Sec. A.6.

4.4. ModelNet40

Relative overlap ratio: We check if PREDATOR focuses on the overlap region. We extract 8,862 test pairs by varying the completeness of the input point clouds from 70 to 40%. As above, we then discard points with a predicted overlap score $o_i < 0.5$, compute the overlap ratio, and compare it to the one of the original scans. Fig. 7 shows that PREDATOR greatly increases the relative overlap and reduces the number of pairs with overlap $< 70\%$ by more than 40 pp.

Comparison to direct registration methods: To be able to compare PREDATOR to RPM-Net [47] and DCP [40], we resort to the synthetic, object-centric dataset they were designed for. We failed to train PRNet [41] due to random crashes of the original code (also observed in [5]).

Remarkably, PREDATOR can compete with methods specifically tuned for *ModelNet*, and in the low-overlap regime outperforms them in terms of *RRE*, see Tab. 4. Moreover, we observe a large boost by sampling points with

Methods	<i>ModelNet</i>			<i>ModelLoNet</i>		
	RRE	RTE	<i>CD</i>	RRE	RTE	<i>CD</i>
DCP-v2 [40]	11.975	0.171	0.0117	16.501	0.300	0.0268
RPM-Net [47]	1.712	0.018	0.00085	<u>7.342</u>	0.124	0.0050
Ours (<i>rand</i>)	2.923	0.034	0.00122	11.585	0.181	0.0104
Ours (<i>prob. (om)</i>)	<u>1.856</u>	<u>0.019</u>	<u>0.00088</u>	5.462	<u>0.133</u>	<u>0.0079</u>

Table 4: Evaluation results on *ModelNet* and *ModelLoNet*. 450 points are sampled for RANSAC with *rand* / *prob.*

overlap attention (*prob. (om)*) rather than randomly (*rand*). Fig. 7 (right) further underlines the importance of sampling in the overlap: PREDATOR is a lot more robust in the low overlap regime ($\approx 8^\circ$ lower RRE at completeness 0.4).

5. Conclusion

We have introduced PREDATOR, a deep model designed for pairwise registration of low-overlap point clouds. The core of the model is an overlap attention module that enables early information exchange between the point clouds’ latent encodings, in order to infer which of their points are likely to lie in their overlap region.

There are a number of directions in which PREDATOR could be extended. At present it is tightly coupled to fully convolutional point cloud encoders, and relies on having a reasonable number of *superpoints* in the bottleneck. Moreover, it builds on the prevalent definition of the overlap region, which counts the fraction of points with a feasible correspondence. This might be a limitation in scenarios where the point density is very uneven. Finally, in future work it would be interesting to explore how our overlap-attention module can be integrated into direct point cloud registration methods, and into other neural architectures that have to handle two or more datasets with low overlap.

References

- [1] Yasuhiro Aoki, Hunter Goforth, Rangaprasad Arun Srivatsan, and Simon Lucey. PointnetLK: Robust & efficient point cloud registration using Pointnet. In *CVPR*, 2019. 3
- [2] K. S. Arun, T. S. Huang, and S. D. Blostein. Least-squares fitting of two 3-d point sets. *IEEE TPAMI*, 9(5):698–700, 1987. 3
- [3] Xuyang Bai, Zixin Luo, Lei Zhou, Hongbo Fu, Long Quan, and Chiew-Lan Tai. D3feat: Joint learning of dense detection and description of 3d local features. In *CVPR*, 2020. 1, 2, 5, 6, 7, 8, 12, 13, 14
- [4] Sungjoon Choi, Qian-Yi Zhou, and Vladlen Koltun. Robust reconstruction of indoor scenes. In *CVPR*, 2015. 1, 11
- [5] Christopher Choy, Wei Dong, and Vladlen Koltun. Deep global registration. In *CVPR*, 2020. 3, 7, 8
- [6] Christopher Choy, JunYoung Gwak, and Silvio Savarese. 4d spatio-temporal convnets: Minkowski convolutional neural networks. In *CVPR*, 2019. 2, 3
- [7] Christopher Choy, Jaesik Park, and Vladlen Koltun. Fully convolutional geometric features. In *ICCV*, 2019. 1, 2, 6, 7, 8, 12, 13, 14
- [8] Brian Curless and Marc Levoy. A volumetric method for building complex models from range images. In *ACM SIGGRAPH*, 1996. 11
- [9] Haowen Deng, Tolga Birdal, and Slobodan Ilic. PPF-FoldNet: Unsupervised learning of rotation invariant 3d local descriptors. In *ECCV*, 2018. 2
- [10] Haowen Deng, Tolga Birdal, and Slobodan Ilic. Ppfnet: Global context aware local features for robust 3d point matching. In *CVPR*, 2018. 2, 11
- [11] Daniel DeTone, Tomasz Malisiewicz, and Andrew Rabinovich. Superpoint: Self-supervised interest point detection and description. In *CVPR Workshops*, 2018. 2
- [12] Mihai Dusmanu, Ignacio Rocco, Tomas Pajdla, Marc Pollefeys, Josef Sivic, Akihiko Torii, and Torsten Sattler. D2-Net: A trainable CNN for joint detection and description of local features. In *CVPR*, 2019. 2
- [13] Justin Gilmer, Samuel S Schoenholz, Patrick F Riley, Oriol Vinyals, and George E Dahl. Neural message passing for quantum chemistry. In *ICML*, 2017. 4
- [14] Zan Gojcic, Caifa Zhou, Jan D Wegner, Leonidas J Guibas, and Tolga Birdal. Learning multiview 3d point cloud registration. In *CVPR*, 2020. 3
- [15] Zan Gojcic, Caifa Zhou, Jan D Wegner, and Andreas Wieser. The perfect match: 3d point cloud matching with smoothed densities. In *CVPR*, 2019. 1, 2, 6, 7, 13
- [16] Zan Gojcic, Caifa Zhou, and Andreas Wieser. Learned compact local feature descriptor for TLS-based geodetic monitoring of natural outdoor scenes. In *ISPRS Annals*, 2018. 2
- [17] Yulan Guo, Mohammed Bennamoun, Ferdous Sohel, Min Lu, Jianwei Wan, and Jun Zhang. Performance evaluation of 3D local feature descriptors. In *ACCV*, 2014. 2
- [18] Maciej Halber and Thomas A. Funkhouser. Structured global registration of RGB-D scans in indoor environments. *arXiv preprint arXiv:1607.08539*, 2016. 11
- [19] A.E. Johnson and M. Hebert. Using spin images for efficient object recognition in cluttered 3d scenes. *IEEE TPAMI*, 21:433–449, 1999. 2
- [20] Marc Khoury, Qian-Yi Zhou, and Vladlen Koltun. Learning compact geometric features. In *ICCV*, 2017. 1, 2, 3
- [21] Kevin Lai, Liefeng Bo, and Dieter Fox. Unsupervised feature learning for 3d scene labeling. In *ICRA*, 2014. 11
- [22] Jonathan Long, Evan Shelhamer, and Trevor Darrell. Fully convolutional networks for semantic segmentation. In *CVPR*, 2015. 2
- [23] Bruce D Lucas and Takeo Kanade. An iterative image registration technique with an application to stereo vision. In *IJCAI*, 1981. 3
- [24] Andrew L Maas, Awni Y Hannun, and Andrew Y Ng. Rectifier nonlinearities improve neural network acoustic models. In *ICML*, 2013. 4
- [25] Vinod Nair and Geoffrey E Hinton. Rectified linear units improve restricted boltzmann machines. In *ICML*, 2010. 4
- [26] Charles R Qi, Hao Su, Kaichun Mo, and Leonidas J Guibas. Pointnet: Deep learning on point sets for 3d classification and segmentation. In *CVPR*, 2017. 2, 3, 5
- [27] Jerome Revaud, Philippe Weinzaepfel, César De Souza, Noe Pion, Gabriela Csurka, Yohann Cabon, and Martin Humenberger. R2D2: Repeatable and reliable detector and descriptor. *arXiv preprint arXiv:1906.06195*, 2019. 2
- [28] Radu Bogdan Rusu, Nico Blodow, and Michael Beetz. Fast point feature histograms (FPFH) for 3D registration. In *ICRA*, 2009. 2
- [29] Radu Bogdan Rusu, Nico Blodow, Zoltan Csaba Marton, and Michael Beetz. Aligning point cloud views using persistent feature histograms. In *IROS*, 2008. 2
- [30] Paul-Edouard Sarlin, Daniel DeTone, Tomasz Malisiewicz, and Andrew Rabinovich. Superglue: Learning feature matching with graph neural networks. In *CVPR*, 2020. 2, 4
- [31] Jamie Shotton, Ben Glocker, Christopher Zach, Shahram Izadi, Antonio Criminisi, and Andrew Fitzgibbon. Scene coordinate regression forests for camera relocalization in RGB-D images. In *CVPR*, 2013. 11
- [32] Richard Sinkhorn. A relationship between arbitrary positive matrices and doubly stochastic matrices. *The annals of mathematical statistics*, 35(2):876–879, 1964. 3
- [33] Yifan Sun, Changmao Cheng, Yuhang Zhang, Chi Zhang, Liang Zheng, Zhongdao Wang, and Yichen Wei. Circle loss: A unified perspective of pair similarity optimization. In *CVPR*, 2020. 5
- [34] Hugues Thomas, Charles R Qi, Jean-Emmanuel Deschaud, Beatriz Marcotequi, François Goulette, and Leonidas J Guibas. KPconv: Flexible and deformable convolution for point clouds. In *CVPR*, 2019. 3
- [35] Federico Tombari, Samuele Salti, and Luigi Di Stefano. Unique shape context for 3D data description. In *ACM Workshop on 3D Object Retrieval*, 2010. 2
- [36] Federico Tombari, Samuele Salti, and Luigi Di Stefano. Unique signatures of histograms for local surface description. In *ECCV*, 2010. 2

- [37] Dmitry Ulyanov, Andrea Vedaldi, and Victor Lempitsky. Instance normalization: The missing ingredient for fast stylization. *arXiv preprint arXiv:1607.08022*, 2016. 4
- [38] Julien Valentin, Angela Dai, Matthias Nießner, Pushmeet Kohli, Philip Torr, Shahram Izadi, and Cem Keskin. Learning to navigate the energy landscape. In *3DV*, 2016. 11
- [39] Ashish Vaswani, Noam Shazeer, Niki Parmar, Jakob Uszkoreit, Llion Jones, Aidan N Gomez, Łukasz Kaiser, and Illia Polosukhin. Attention is all you need. In *NeurIPS*, 2017. 4
- [40] Yue Wang and Justin M Solomon. Deep closest point: Learning representations for point cloud registration. In *ICCV*, 2019. 2, 3, 8
- [41] Yue Wang and Justin M Solomon. PRNet: Self-supervised learning for partial-to-partial registration. In *NeurIPS*, 2019. 2, 3, 7, 8
- [42] Yue Wang, Yongbin Sun, Ziwei Liu, Sanjay E Sarma, Michael M Bronstein, and Justin M Solomon. Dynamic graph CNN for learning on point clouds. *ACM TOG*, 38(5), 2019. 3
- [43] Olivia Wiles, Sebastien Ehrhardt, and Andrew Zisserman. D2D: Learning to find good correspondences for image matching and manipulation. *arXiv preprint arXiv:2007.08480*, 2020. 2
- [44] Zhirong Wu, Shuran Song, Aditya Khosla, Fisher Yu, Linguang Zhang, Xiaoou Tang, and Jianxiong Xiao. 3d shapenets: A deep representation for volumetric shapes. In *CVPR*, 2015. 6
- [45] Jianxiong Xiao, Andrew Owens, and Antonio Torralba. Sun3d: A database of big spaces reconstructed using sfm and object labels. In *ICCV*, 2013. 11
- [46] Zi Jian Yew and Gim Hee Lee. 3dfeat-net: Weakly supervised local 3d features for point cloud registration. In *ECCV*, pages 630–646. Springer, 2018. 2
- [47] Zi Jian Yew and Gim Hee Lee. RPM-Net: Robust point matching using learned features. In *CVPR*, 2020. 3, 6, 7, 8, 11
- [48] Andy Zeng, Shuran Song, Matthias Nießner, Matthew Fisher, Jianxiong Xiao, and Thomas Funkhouser. 3DMatch: learning local geometric descriptors from RGB-D reconstructions. In *CVPR*, 2017. 1, 2, 3, 6, 11

A. Supplementary material

In this supplementary material, we first provide rigorous definitions of evaluation metrics (Sec. A.1), then describe the data pre-processing step (Sec. A.2), network architectures (Sec. A.3) and training on *ModelNet40* (Sec. A.4) in more detail. We further provide additional results (Sec. A.5), ablation studies (Sec. A.6) as well as a runtime analysis (Sec. A.7). Finally, we show more visualisations on *3DLoMatch* and *ModelLoNet* benchmarks (Sec. A.8).

A.1. Evaluation metrics

The evaluation metrics, which we use to assess model performance in Sec. 4 of the main paper and Sec. A.5 of this supplementary material, are formally defined as follows:

Inlier ratio looks at the set of putative correspondences $(\mathbf{p}, \mathbf{q}) \in \mathcal{K}_{ij}$ found by reciprocal matching⁶ in feature space, and measures what fraction of them is "correct", in the sense that they lie within a threshold $\tau_1 = 10$ cm after registering the two scans with the ground truth transformation $\bar{T}_{\mathbf{P}}^{\mathbf{Q}}$:

$$\text{IR} = \frac{1}{|\mathcal{K}_{ij}|} \sum_{(\mathbf{p}, \mathbf{q}) \in \mathcal{K}_{ij}} [\|\bar{T}_{\mathbf{P}}^{\mathbf{Q}}(\mathbf{p}) - \mathbf{q}\|_2 < \tau_1], \quad (12)$$

with $[\cdot]$ the Iverson bracket.

Feature Match recall (FMR) [10] measures the fraction of point cloud pairs for which, based on the number of inlier correspondences, it is *likely* that accurate transformation parameters can be recovered with a robust estimator such as RANSAC. Note that FMR only checks whether the inlier ratio is above a threshold $\tau_2 = 0.05$. It does not test if the transformation can actually be determined from those correspondences, which in practice is not always the case, since their geometric configuration may be (nearly) degenerate, e.g., they might lie very close together or along a straight edge. A single pair of point clouds counts as suitable for registration if

$$\text{IR} > \tau_2 \quad (13)$$

Registration recall [4] is the most reliable metric, as it measures end-to-end performance on the actual task of point cloud registration. Specifically, it looks at the set of ground truth correspondences \mathcal{H}_{ij}^* after applying the estimated transformation $T_{\mathbf{P}}^{\mathbf{Q}}$, computes their root mean square error,

$$\text{RMSE} = \sqrt{\frac{1}{|\mathcal{H}_{ij}^*|} \sum_{(\mathbf{p}, \mathbf{q}) \in \mathcal{H}_{ij}^*} \|T_{\mathbf{P}}^{\mathbf{Q}}(\mathbf{p}) - \mathbf{q}\|_2^2}, \quad (14)$$

and checks for what fraction of all point pairs $\text{RMSE} < 0.2$. In keeping with the original evaluation script of *3DMatch*,

⁶We follow *3DMatch* [48] and apply reciprocal matching as a pre-filtering step.

immediately adjacent point clouds are excluded, since they have very high overlap by construction.

Chamfer distance measures the quality of registration on synthetic data. We follow [47] and use the *modified* Chamfer distance metric:

$$\begin{aligned} \tilde{CD}(\mathbf{P}, \mathbf{Q}) = & \frac{1}{|\mathbf{P}|} \sum_{\mathbf{p} \in \mathbf{P}} \min_{\mathbf{q} \in \mathbf{Q}_{\text{raw}}} \|T_{\mathbf{P}}^{\mathbf{Q}}(\mathbf{p}) - \mathbf{q}\|_2^2 + \\ & \frac{1}{|\mathbf{Q}|} \sum_{\mathbf{q} \in \mathbf{Q}} \min_{\mathbf{p} \in \mathbf{P}_{\text{raw}}} \|\mathbf{q} - T_{\mathbf{P}}^{\mathbf{Q}}(\mathbf{p})\|_2^2 \end{aligned} \quad (15)$$

where $\mathbf{P}_{\text{raw}} \in \mathbb{R}^{2048 \times 3}$ and $\mathbf{Q}_{\text{raw}} \in \mathbb{R}^{2048 \times 3}$ are *raw* source and target point clouds, $\mathbf{P} \in \mathbb{R}^{717 \times 3}$ and $\mathbf{Q} \in \mathbb{R}^{717 \times 3}$ are *input* source and target point clouds.

Relative translation and rotation errors (RTE/RRE) measure the deviations from the ground truth pose as:

$$\begin{aligned} \text{RTE} &= \|\mathbf{t} - \bar{\mathbf{t}}\|_2 \\ \text{RRE} &= \arccos\left(\frac{\text{trace}(\mathbf{R}^T \bar{\mathbf{R}}) - 1}{2}\right) \end{aligned} \quad (16)$$

where \mathbf{R} and \mathbf{t} denote the estimated rotation matrix and translation vector, respectively.

A.2. Dataset preprocessing

3DMatch: This is a collection of 62 scenes, combining earlier data from Analysis-by-Synthesis [38], 7Scenes [31], SUN3D [45], RGB-D Scenes v.2 [21], and Halber *et al.* [18]. The official specifications split the data into 54 scenes for training and 8 for testing. Individual scenes are not only captured in different indoor spaces (e.g., bedrooms, offices, living rooms, restrooms) but also with different depth sensors (e.g., Microsoft Kinect, Structure Sensor, Asus Xtion Pro Live, and Intel RealSense). *3DMatch* provides great diversity and allows our model to generalize across different indoor spaces. Individual scenes of *3DMatch* are split into point cloud fragments, which are generated by fusing 50 consecutive depth frames using TSDF volumetric fusion [8]. As a preprocessing step, we apply voxel-grid downsampling to all point clouds, and if multiple points fall into the same voxel, we randomly pick one.

ModelNet40: For each CAD model, 2048 points are first generated by uniform sampling and scaled to fit into a unit sphere. Then we follow [47] to produce partial scans: for source partial point cloud, we uniformly sample a plane through the origin that splits the unit sphere into two half-spaces, shift that plane along its normal until $\lfloor 2048 \cdot p_v \rfloor$ points are on one side, and discard the points on the other side; the target point cloud is generated in the same manner; then the two resulting, partial point clouds are randomly rotated, translated and jittered with Gaussian noise. For the rotation, we sample a random axis and a random angle

	# strided convolutions	convolution radius	first conv. feature dim.	final feature dim.
<i>3DMatch</i>	3	2.5	64	32
<i>ModelNet</i>	2	2.75	256	96

Table 5: Different network configurations for *3DMatch* and *ModelNet* datasets.

$<45^\circ$. The translation is sampled in the range $[-0.5, 0.5]$. Gaussian noise is applied per coordinate with $\sigma = 0.05$. Finally, 717 points are randomly sampled from the $[2048 \cdot p_v]$ points.

A.3. Network architecture

The detailed network architecture of PREDATOR is depicted in Fig. 9. Our model is built on the KPConv implementation from the D3Feat repository.⁷ We complement each KPConv layer with instance normalisation Leaky ReLU activations. The l -th strided convolution is applied to a point cloud downsampled with voxel size $2^l \cdot V$. Upsampling in the decoder is performed by querying the associated feature of the closest point from the previous layer.

With $\approx 20k$ points after voxel-grid downsampling, the point clouds in *3DMatch* are much denser than those of *ModelNet40* with only 717 points. Moreover, they also have larger spatial extent with bounding boxes up to $3 \times 3 \times 3 \text{ m}^3$, while *ModelNet40* point clouds are normalised to fit into a unit sphere. To account for these large differences, we slightly adapt the encoder and decoder per dataset, but keep the same overlap attention model. Differences in network hyper-parameters are shown in Tab. 5.

A.4. Implementation and training

This section complements Sec. 3.5 of the main paper, where implementation and training details are described only for *3DMatch*. Here, we provide those details for *ModelNet40*.

We train PREDATOR on *ModelNet40* for 200 epochs, using SGD with initial learning rate 0.01, momentum 0.98, and weight decay 10^{-6} . The learning rate is exponentially decayed by a factor of 0.95 after each epoch. We use batch size 1, but accumulate gradients over 4 steps. Similar to *3DMatch*, the matchability loss is added when $>30\%$ of points in the overlap region can be matched correctly. Due to the sparsity of *ModelNet*, the input point clouds are not voxel-grid downsampled before the first convolution layer. In the strided convolutions, the voxel size V is set to 0.06. For the circle loss, the positive radius r_p is set to 0.018, the safe radius is 0.06. For overlap loss and matchability loss, r_o and r_m are both set to 0.04. RANSAC is run for 50,000 iterations, with distance threshold $0.5 \cdot r_m$.

⁷<https://github.com/XuyangBai/D3Feat.pytorch>

A.5. Additional results

Detailed registration results: We report detailed per-scene *Registration Recall (RR)*, *Relative Rotation Error (RRE)* and *Relative Translation Error (RTE)* in Tab. 6. RRE and RTE are only averaged over successfully registered pairs for each scene, such that the numbers are not dominated by gross errors from complete registration failures. We get the highest RR and lowest or second lowest RTE and RRE for almost all scenes, this further shows that our overlap attention module together with probabilistic sampling supports not only robust, but also accurate registration.

Feature match recall: Finally, Fig. 8 shows that our descriptors are robust and perform well over a wide range of thresholds for the allowable inlier distance and the minimum inlier ratio. Notably, PREDATOR consistently outperforms D3Feat that uses a similar KPConv backbone.

A.6. Additional ablation studies

Ablations of overlap attention module: We compare PREDATOR with a baseline model, which is a plain encoder-decoder architecture based on KPConv, without the proposed overlap attention module. It outputs 32-dimensional features without overlap and matchability scores. In the absence of those scores, we randomly sample 5,000 points and pass them to RANSAC for registration. As shown in Tab. 7, this baseline model achieves the second highest FMR on two benchmarks, but only reaches 82.5% and 38.9% RR on *3DMatch* and *3DLoMatch* respectively; much worse than the four other variants that include (at least) the overlap score. The experiment again confirms that high FMR or IR does not imply high RR, and thus good registration performance.

Ablations of matchability score: We find that probabilistic sampling guided by the product of the overlap and matchability scores attains the highest RR. Here we further analyse the impact of each individual component. We first construct a baseline which applies random sampling (*rand*) over conditioned features, then we sample points with probability proportional to overlap scores (*prob. (o)*), to matchability scores (*prob. (m)*), and to the combination of the two scores (*prob. (om)*). As shown in Tab. 8, *rand* fares clearly worse, in all metrics. Compared to *prob. (om)*, either *prob. (o)* or *prob. (m)* can achieve comparable results on *3DMatch*; the performance gap becomes big on the more challenging *3DLoMatch* dataset, where our *prob. (om)* is around 4 pp better in terms of RR.

A.7. Timings

We compare the runtime of PREDATOR with FCGF⁸ [7] and D3Feat⁹ [3] on *3DMatch*. For all three methods we

⁸All experiments were done with MinkowskiEngine v0.4.2.

⁹We use its PyTorch implementation.

3DMatch											3DLoMatch										
	Kitchen	Home 1	Home 2	Hotel 1	Hotel 2	Hotel 3	Study	MIT Lab	Avg.	STD		Kitchen	Home 1	Home 2	Hotel 1	Hotel 2	Hotel 3	Study	MIT Lab	Avg.	STD
# Sample																					
	449	106	159	182	78	26	234	45	160	128		524	283	222	210	138	42	237	70	191	154
Registration Recall (%)																					
3DSN [15]	90.6	90.6	65.4	89.6	82.1	80.8	68.4	60.0	78.4	11.5		51.4	25.9	44.1	41.1	30.7	36.6	14.0	20.3	33.0	11.8
FCGF [7]	98.0	94.3	68.6	96.7	91.0	84.6	76.1	71.1	85.1	11.0		60.8	42.2	53.6	53.1	38.0	26.8	16.1	30.4	40.1	14.3
D3Feat [3]	96.0	86.8	67.3	90.7	88.5	80.8	78.2	64.4	81.6	10.5		49.7	37.2	47.3	47.8	36.5	31.7	15.7	31.9	37.2	10.6
Ours	97.1	96.2	73.6	96.7	94.9	84.6	85.9	77.8	88.3	8.7		66.3	58.9	55.0	71.8	57.7	46.3	39.8	37.7	54.2	11.4
Relative Rotation Error (°)																					
3DSN [15]	1.926	1.843	2.324	2.041	1.952	2.908	2.296	2.301	2.199	0.321		3.020	3.898	3.427	3.196	3.217	3.328	4.325	3.814	3.528	0.414
FCGF [7]	1.767	1.849	2.210	1.867	1.667	2.417	2.024	1.792	1.949	0.236		2.904	3.229	3.277	2.768	2.801	2.822	3.372	4.006	3.147	0.394
D3Feat [3]	2.016	2.029	2.425	1.990	1.967	2.400	2.346	2.115	2.161	0.183		3.226	3.492	3.373	3.330	3.165	2.972	3.708	3.619	3.361	0.227
Ours	1.859	1.808	2.373	1.816	1.825	2.315	2.047	1.926	1.996	0.214		3.225	3.017	3.183	3.013	3.165	3.421	3.446	2.873	3.168	0.186
Relative Translation Error (m)																					
3DSN [15]	0.059	0.070	0.079	0.065	0.074	0.062	0.093	0.065	0.071	0.010		0.082	0.098	0.096	0.101	0.080	0.089	0.158	0.120	0.103	0.024
FCGF [7]	0.053	0.056	0.071	0.062	0.061	0.055	0.082	0.090	0.066	0.013		0.084	0.097	0.076	0.101	0.084	0.077	0.144	0.140	0.100	0.025
D3Feat [3]	0.055	0.065	0.080	0.064	0.078	0.049	0.083	0.064	0.067	0.011		0.088	0.101	0.086	0.099	0.092	0.075	0.146	0.135	0.103	0.023
Ours	0.051	0.062	0.072	0.059	0.062	0.049	0.078	0.079	0.064	0.011		0.081	0.091	0.075	0.093	0.098	0.091	0.114	0.087	0.091	0.011

Table 6: Detailed results on the 3DMatch and 3DLoMatch datasets.

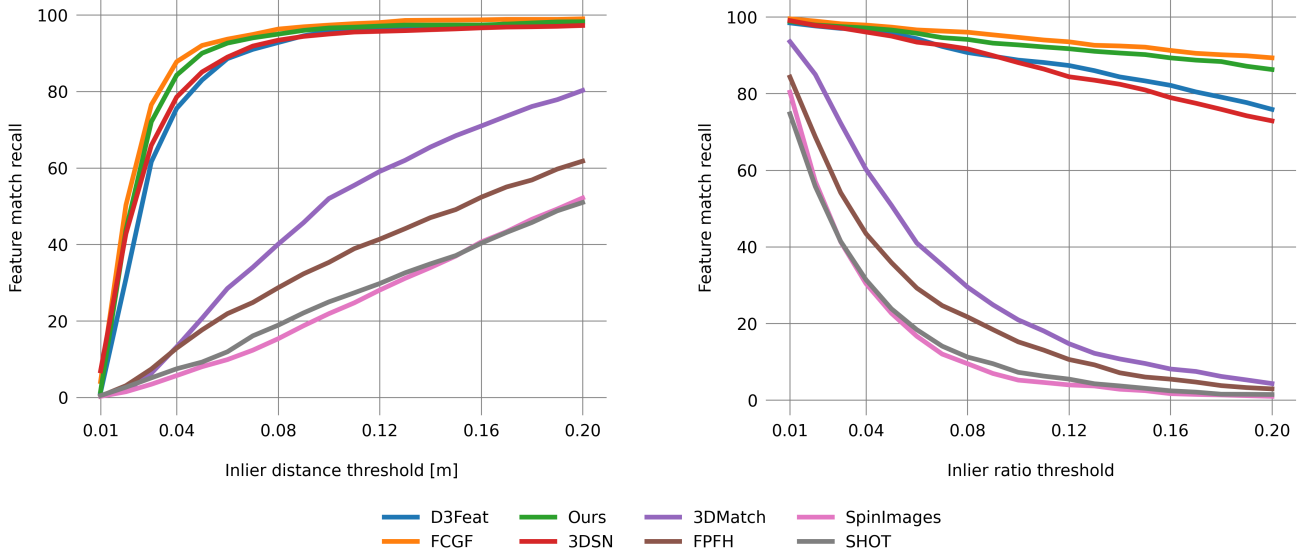


Figure 8: Feature matching recall in relation to inlier distance threshold τ_1 (left) and inlier ratio threshold τ_2 (right)

set voxel size $V = 2.5$ cm and batch size 1. The test is run on a single GeForce GTX 1080 Ti with Intel(R) Core(TM) i7-7700K CPU @ 4.20GHz, 32GB RAM. The most time-consuming step of our model, and also of D3Feat, is the data loader, as we have to pre-compute the neighborhood indices before the forward pass. With its smaller encoder and decoder, but the additional overlap attention module, PREDATOR is still marginally faster than D3Feat. FCGF has a more efficient data loader that relies on sparse convolution and queries neighbors during the forward pass. See Tab. 9.

A.8. Qualitative visualization

We show more qualitative results in Fig. 10 and Fig. 11 for 3DLoMatch and ModelLoNet respectively. The input

points clouds are rotated and translated here for better visualization of overlap and matchability scores.

overlap attention			<i>3DMatch</i>			<i>3DLoMatch</i>		
<i>ov.</i>	$\times ov.$	<i>cond.</i>	FMR	IR	RR	FMR	IR	RR
			<u>96.4</u>	39.6	82.6	<u>72.2</u>	14.5	38.9
✓			96.2	47.2	86.9	71.8	<u>18.0</u>	50.9
✓	✓		96.1	<u>47.8</u>	<u>87.3</u>	69.5	15.8	48.4
✓		✓	95.5	46.4	87.1	73.0	17.6	54.4
✓	✓	✓	96.6	49.9	88.3	71.7	20.0	<u>54.2</u>

Table 7: Ablation of the network architecture design; *ov.* denotes upsampling the overlap scores, *cond.* denotes conditioning the bottleneck features on the respective other point cloud, $\times ov.$ denotes that the cross overlap scores is also appended to the features as input to the decoder.

matchability	overlap	<i>3DMatch</i>			<i>3DLoMatch</i>		
		FMR	IR	RR	FMR	IR	RR
		96.0	43.6	83.9	69.3	15.7	39.3
✓		<u>96.3</u>	<u>48.4</u>	87.8	72.2	<u>19.4</u>	<u>50.8</u>
	✓	96.1	46.2	<u>88.0</u>	71.3	16.9	49.3
✓	✓	96.6	49.9	88.3	<u>71.7</u>	20.0	54.2

Table 8: Different combinations of scores used for probabilistic sampling.

	data loader	encoder	overlap attention	decoder	overall
FCGF [7]	6	414	—	25	445
D3Feat [3]	200	<u>11</u>	—	<u>63</u>	<u>274</u>
Ours	<u>191</u>	9	70	1	271

Table 9: Runtime per fragment in milli-seconds, averaged over 1623 test pairs of *3DMatch*.

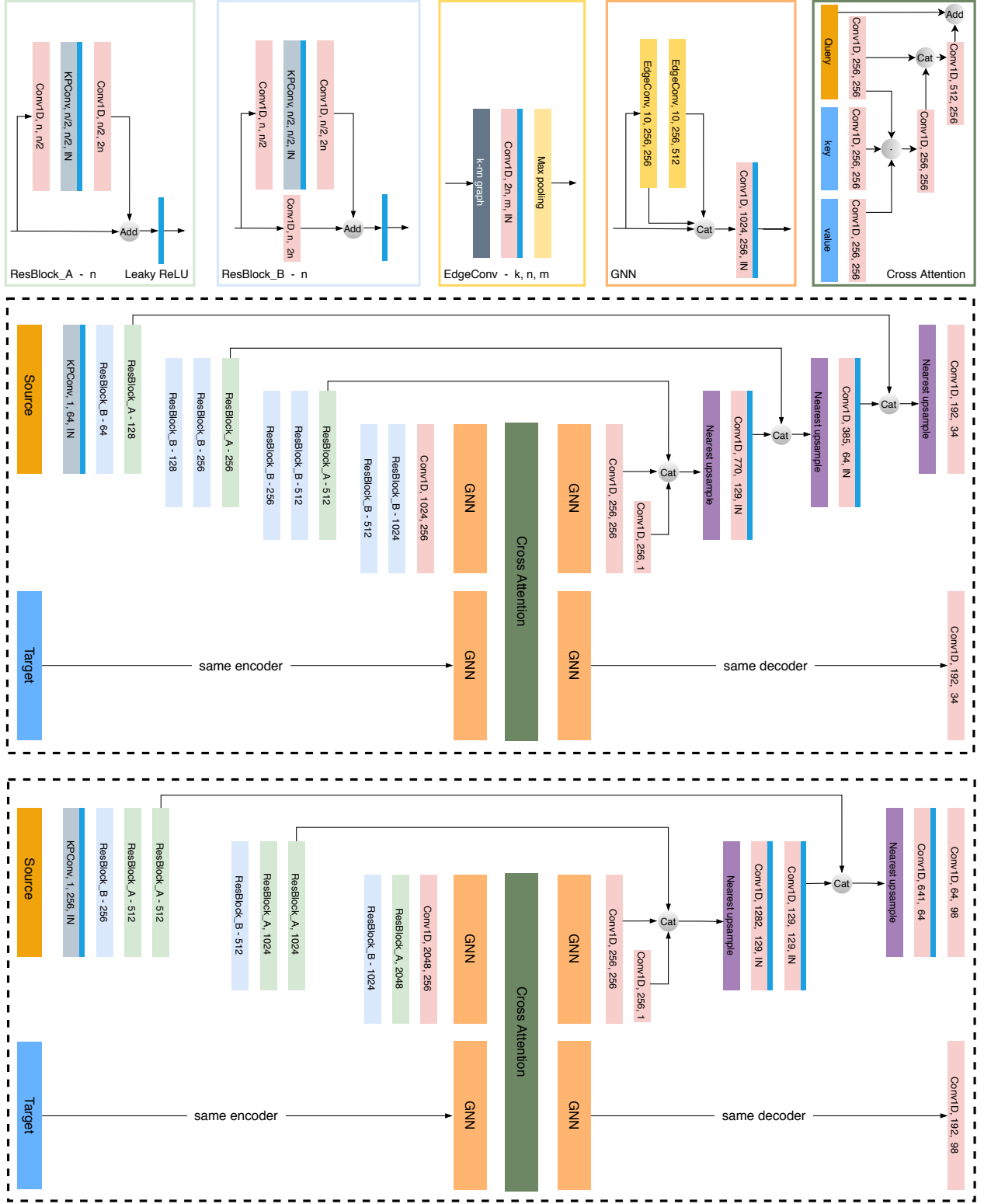


Figure 9: Network architecture of PREDATOR for 3DMatch (middle) and ModelNet (bottom). In the cross attention module, for each (query $s_i \in \mathbb{R}^{b \times 1}$, key $k_i \in \mathbb{R}^{b \times 1}$, value $v_i \in \mathbb{R}^{b \times 1}$), \odot denotes first reshape them into shape $(4, \frac{b}{4})$ (4 heads), then compute scores matrix S from s_i and k_i , finally get message update from v_i and reshape back to $(b, 1)$.

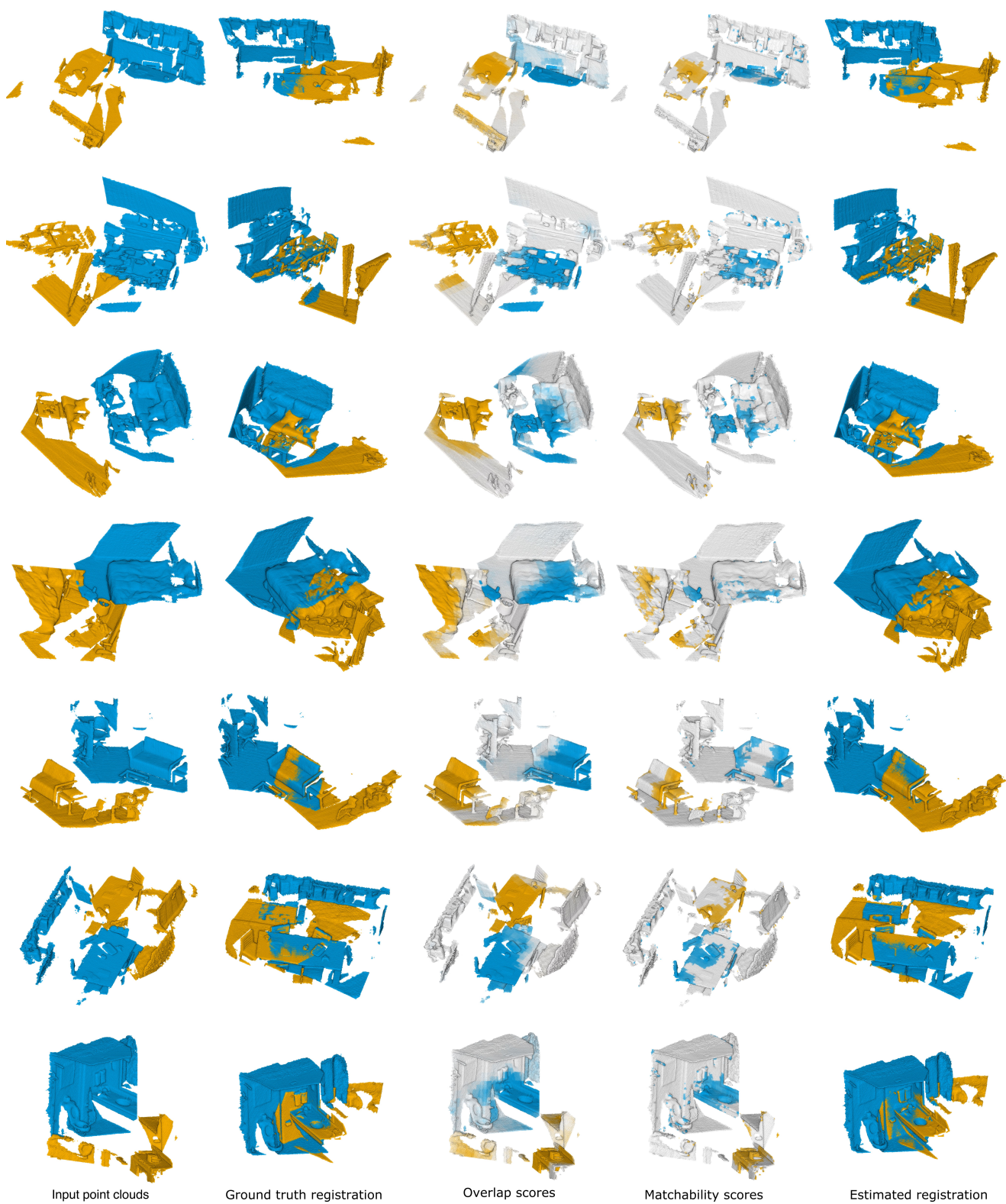


Figure 10: Example results on *3DLoMatch*.

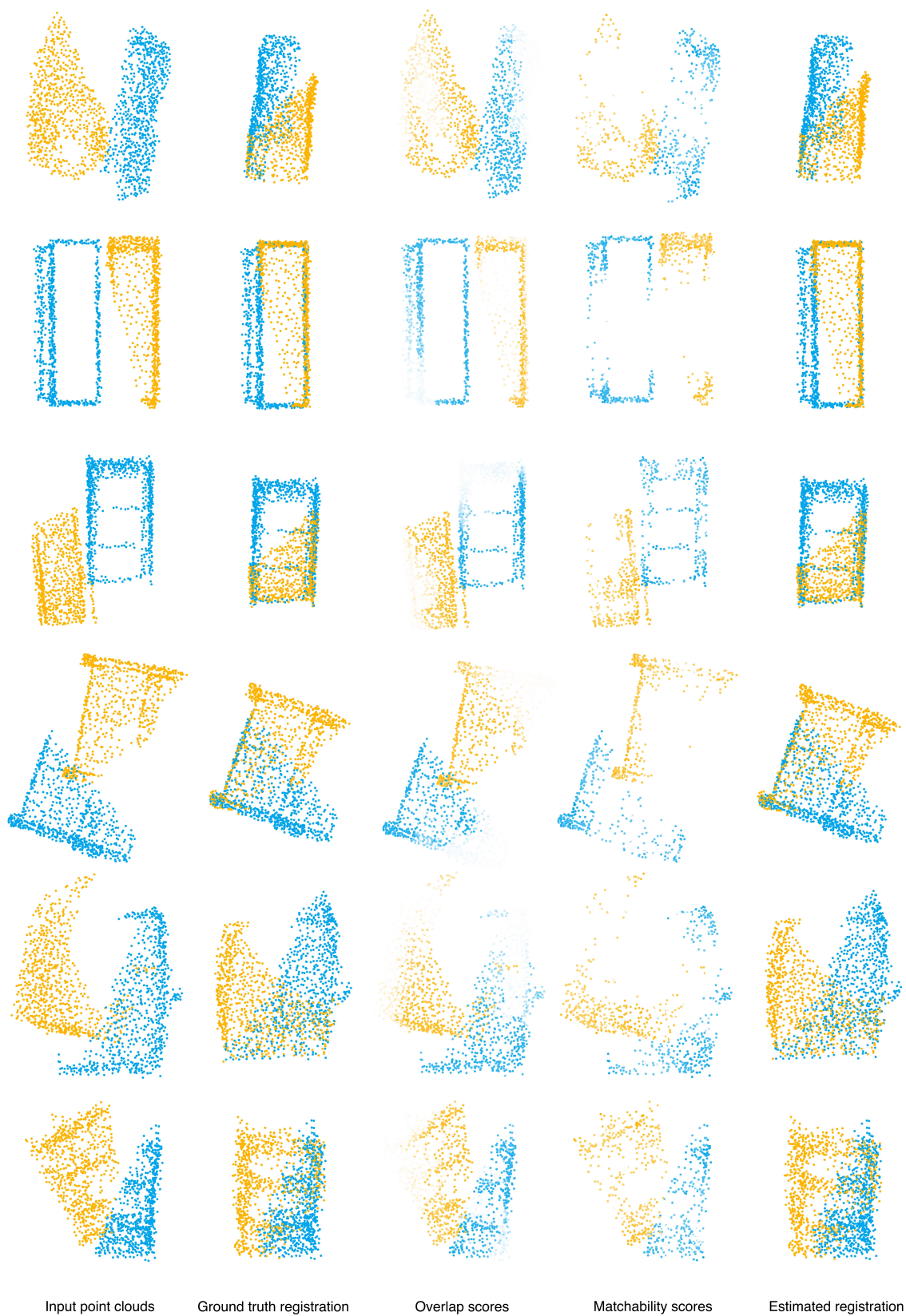


Figure 11: Example results on *ModelLoNet*.